

# Effect of the Euclidean dimensionality on the energy transfer up-conversion luminescence

Leopoldo Mejía<sup>a,b</sup>, C.Z. Hadad<sup>a,\*</sup>

<sup>a</sup> Instituto de Química, Universidad de Antioquia, Calle 70 No. 52-21, Medellín, Colombia

<sup>b</sup> Department of Chemistry, University of Rochester, Rochester, New York, 14627-0216, USA

## ARTICLE INFO

### Keywords:

Energy transfer up-conversion  
Material dimensionality  
Analytical model  
Transient luminescence  
Optical centers

## ABSTRACT

An analytical model to study the influence of the Euclidian spatial dimensionality of the medium on the transient luminescence produced exclusively by up-conversion energy transfer interaction among randomly distributed optical centers is developed. The model is intrinsically coherent in terms of the coordinated behavior of the relevant states luminescence and of the macroscopic energy transfer rate, and shows agreement with expected general trends. Its predictions indicate that, under comparable conditions, the rate of the up-conversion follows the  $1D > 2D > 3D$  tendency at initial times, but that this conduct reverses at some (concentration and pump power independent) time point, resulting in a higher total up-conversion luminescence for larger dimensionalities. The model predicts that under continuous excitation regime higher up-conversion luminescence is expected for smaller Euclidean dimensions. Finally, the study also shows that up-conversion luminescence is very sensitive to the value of the minimum possible distance of optical centers mutual approach,  $R_m$ , especially in low-dimensional medium, and not considering it -as traditionally occurs in the analysis of other energy transfer processes- induces to inaccuracies in the observables description.

## 1. Introduction

An event of energy transfer up-conversion, ETU [1,2], occurs when some optical center (donor) transfers excitation energy to another optical center (acceptor) that is already in some excited state. The same acceptor may undergo several times this process, which can also be accompanied by other photophysical phenomena [1,2]. As a result of the up-conversion process, the acceptor reaches higher excited states, from where it can decay radiatively, emitting light that is of higher frequency than the one (or its equivalent in energy) used to excite the substance.

As expected, this phenomenon has many possibilities of technological application [2–8]. For example, it has been used to map biological processes and bio-structures; nanoparticles or other structures or substances, containing the appropriate optical centers, are introduced into the tissue or in a biological-like system and excited with light of penetrating wavelength, for example IR, which is converted by the substance into VIS or UV light, which can be detected by naked eye or with some instruments, and thus unveiling the process or structure under study [7,9]. Likewise, with this technique has emerged the possibility of specific manipulation of membrane ion channels, the so called up-conversion optogenetics [10], which opens a wide range of options for

the control of physiological and pathophysiological processes. Other relevant examples of uses are in visible solid state lasers [11], in specific thermometry [4,12], in display devices [13,14], and in many others in the field of photonics, imaging, biotechnology, nanomedicine, etc. In particular, the ETU process has potential applications in fields where the simple energy transfer, ET, process (traditional Förster Energy Transfer, FRET [15–17]) already had, for example, as spectroscopic rule in biochemistry and biophysics [6,15–17]. In fact, in recent years, the amount of experimental research about new materials and new possibilities for the up-conversion uses is so overwhelming, that it has been a subject of special issues in prestigious journals (see, for example, Bergamini and Ceroni [18]).

Like any usual ET process, the general requirement for each ETU event is that the energy gap involved in the donor transition roughly matches that of the acceptor transition [1,2,15]. This requirement is fulfilled by a series of optical centers combinations consisting of inorganic ions, organic molecules, semiconductors, and composite entities [1–15,18]. Electronic transitions between states originated from f orbitals in trivalent lanthanides,  $\text{Ln}^{3+}$ , are among the most interested [1,2,19]. Although f-f transitions are prohibited and, with this, of limited absorption and emission probabilities, they are very attractive from the technological point of view;  $\text{Ln}^{3+}$  luminescence has relatively long

\* Corresponding author.

E-mail address: [cacier.hadad@udea.edu.co](mailto:cacier.hadad@udea.edu.co) (C.Z. Hadad).

<https://doi.org/10.1016/j.jphotochem.2019.111908>

Received 2 March 2019; Received in revised form 20 May 2019; Accepted 3 June 2019

Available online 05 June 2019

1010-6030/ © 2019 Elsevier B.V. All rights reserved.

lifetimes, very narrow emission wavelength ranges (f orbitals are internal ones and their participation in bonding is quite small, so vibronic couplings are low), and the variety of atoms in the lanthanide series, with different dispositions of  $\text{Ln}^{3+}$  energy levels, and with transition possibilities ranging from IR to UV, passing through the VIS, allows many options for the design of materials with desired properties [19]. In addition,  $\text{Ln}^{3+}$  can be incorporated into many types of crystalline, amorphous, organic and inorganic matrices, in supra-structures, forming part of coordination compounds, etc. All this makes them very versatile for the design of optical devices [19].

With respect to the architecture and size of optical centers host matrices, apart from the core-shell nanometric very useful design [20], in the last decades there has been an upswing in the synthesis of miniaturized materials with Euclidean dimensions different from three (3D), such as two-dimensional (2D) sheets, plates, films, etc. [21–26], one-dimensional (1D) wires, bars, tubes, rods, etc [27–32], with thicknesses and diameters ranging from units to hundreds of nanometers, mainly of crystalline inorganic nature. For reasons that relates the nano form of the material with its area/volume ratio, its structural defects, the mutual proximity of its dopant optical centers, and its electronic structure, its luminescent properties are enhanced with respect to the ones of conventional materials. Additionally, nano-sizes and low Euclidean dimensions provide several advantages in terms of use possibilities [21–32].

Given the even greater improvements in the methodologies of material synthesis and analysis, and the technological advances oriented to the miniaturization and the confinement at molecular scale, in the last times the interest in materials and systems capable of housing or disposed molecules or ions in true 1D and 2D architectures (spaces or structures of diameter (1D) or thickness (2D) of around or less than 1 nm) is growing [33–50]. Consequently, it is valid to ask about the possibility of having optical centers structured and/or confined in these restricted dimensions. Indeed, ET [36–39,45–49] and even ETU [37,38,40,41] events have been observed in true 1D and 2D architectures. In those studies it is reported that the structuring of molecules in 1D or 2D allows the introduction of some desired luminescent properties, or also that the confinement in true 1D or 2D introduces improvements in the observed luminescence, and the optimization and tuning capacity in the energy transfer efficiency [36–41,45–49].

In view of these new scenarios for photonic science and technology of reduced dimensions, it is valid to ask: what general physical characteristics would have the up-conversion luminescence originated by energy transfer in 1D and 2D, and what difference would there be with respect to the classic 3D case? To get a general answer, we have to set general conditions for the studied system. Therefore, the main goal of this paper is to study the effects of the reduction of the medium's dimensionality on the up-conversion luminescence caused by randomly distributed optical centers. For this it is convenient to build a model that relates a basic ETU scheme (without other accompanying processes) to the dimensionality of the medium, incorporating some general structural factor that accounts for the particularities of each system. The sufficiently general structural factor can be the minimum possible approach distance between two optical centers,  $R_m$ , which will change with the nature of each luminophore and/or of the hosting medium. It is necessary to emphasize that, precisely because it is oriented to the direct and simple study of the effect of dimensionality on ETU, our model will have several approximations and, in most cases, it is not applicable in its current version to the analysis of experimental curves. To be applicable, it is necessary to incorporate, at least, the energy migration process. A more complete development to be used in experimental analysis is necessarily more complex and inconvenient for the purposes of this study (such development is in progress and will be published elsewhere).

Although, to our knowledge, there are no theoretical models that describe the general influence of Euclidean dimensionality on the time dependent up-conversion luminescence, the problem of simple ET in

restricted dimensions and geometries had already been addressed theoretically [51–58]. This was mainly encouraged by the fact that biochemical processes occur very frequently in 2D membranes and unidimensional structures, and with FRET-based techniques it is possible to study them [9,17,51,52]. Not only this, but also due to the study of 3D crystalline structures with 1D and 2D subdomains [56,59,60], structures with characteristics of fractals or porous media [53,54], etc. In what follows, we will mention some models having relevant elements for our study. One of the first models for simple ET in 2D is that of Wolber and Hudson, who proposed a Förster-like analysis for randomly distributed donors and acceptors in a plane, considering dipole-dipole interaction [51]. The model was successfully applied to describe the fluorescence of a membrane-bound donor by membrane-bound acceptors. Snyder and Freire developed a Monte Carlo sampling-based model to quantitatively study the dipole-dipole ET quenching in a 2D non-ideal mixing of lipid and protein, and the effect of excluded volume and lattice structures on the expected transfer efficiencies [52]. The results clearly showed the utility of energy transfer-based techniques and its theoretical analysis to obtain organizational parameters that accurately reflect the distribution of protein and lipid molecules within a bilayer membrane. On the other hand, Klafter and Blumen developed an analytical model for any multipolar interaction and any dimensionality of the medium to study more general cases of trapping and reaction processes on fractals of any dimension, which include simple ET processes in 1, 2, and 3 dimensions. The model allows its application and extension in restricted geometries, such as, for example, different porous structures [54], but, as indicated by Klafter and Blumen [54] and other authors [17,57], it should be used with care so as not to misinterpret the results about the dimensionality of the system. For its part, Vásquez [56] applied the so called Crystal Model for analyzing the simple ET in quasi-bidimensional structures for multipolar and exchange interactions, finding that the model allows to account for the observed change, between  $\text{Na}_2\text{Gd}_2\text{xEu}_{2(1-x)}\text{Ti}_3\text{O}_{10}$  and  $\text{NaGd}_x\text{Eu}_{(1-x)}\text{TiO}_4$  systems, in the critical optical centers concentration for the quenching of the  $^5\text{D}_0 \rightarrow ^7\text{F}_2$  emission. Additionally, the analysis allowed to determine that in these lanthanide-based systems the dominant interaction is of the dipole-dipole type.

The basic form of the Förster-like models described above for simple ET [51,53–55] can be synthesized in an expression for the transient intensity of the donor luminescence,  $I_D(t)$ , deactivated by randomly distributed acceptors in infinite media of dimension  $d = 1, 2, 3$  [17,53,55]:

$$I_D(t) = I_D(0) \times e^{-kt} \times e^{-C_A V_d R_0^d \Gamma\left(1 - \frac{d}{s}\right) (kt)^{\frac{d}{s}}} \quad (1)$$

where  $t$  is the time,  $k$  is the donor deactivation rate in the absence of the acceptor (the inverse of the lifetime of the donor),  $C_A$  the numerical concentration of the acceptor,  $V_d R_0^d$  the capacity of the medium of dimension  $d$ , in a radius of Förster  $R_0$ ; a volume,  $\frac{4\pi}{3} R_0^3$ , an area,  $\pi R_0^2$ , or a length,  $2R_0$  [17,53,55],  $\Gamma(x)$  is the Gamma function, and  $s$  is the interaction multipole.

Now, considering our main goal (described above), is the model of Eq. (1) compatible with a theoretical Förster-like treatment for up-conversion luminescence? How to incorporate  $R_m$  in the description of the up-conversion luminescence? Does  $R_m$  really play an important role for up-conversion? Wolber and Hudson model [51] gives us some insight about the incorporation of  $R_m$  into a Förster-like theoretical treatment. Additionally, we previously developed a model for up-conversion in 3D that incorporates  $R_m$  [61,62]. However, given the approximations in its development [61], this model contains only partial descriptions in regions where  $R_m$  is relevant (Near initial time) and is a model not directly applicable to Euclidean dimensions different from 3. The model developed here to answer these questions will also be based on a general Förster-like treatment for multipolar interactions (otherwise, the most common) and, therefore, must also account for the Eq. (1) in the limit of its validity.

Although the parameters used in the results and discussions section of this paper are representative of materials containing  $\text{Ln}^{3+}$ , the model and conceptual conclusions to be presented will have universal validity, and, for example, can be taken into consideration for analysis of dimensionality effects in systems containing organic optical centers, or in biological systems with optical centers randomly distributed in 1D structures, 2D membranes, or in 3D fluid media, where, depending on the viscosity of the medium, the so called *static limit* [17] for ET can be met.

## 2. Model

This work will be based on the simplified ETU process schematized in Fig. 1. Two generic optical centers,  $i$  and  $j$ , of similar electronic characteristics are initially in the intermediate state, (2), reached after selective excitation with a laser pulse of intensity,  $I$ . Once there, optical centers have the possibility of radiative/non-radiative intra-center decay to any lower state (for simplicity, Fig. 1 only shows the decay to the ground state), with rate constant  $k_2$ , or of carrying out the ETU process, with rate  $W(r_{ij})$  [1,53],

$$W(r_{ij}) = \frac{\Omega_s}{r_{ij}^s} \quad (2)$$

where  $\Omega_s$  is a parameter that can be expressed completely in terms of spectroscopic observables or in terms of the Förster critical transfer distance [1,63,64],  $r_{ij}$  is the distance between  $i$  and  $j$ , and  $s = 6, 8, 10$  for dipole-dipole, dipole-quadrupole and quadrupole-quadrupole interactions, respectively [1,63–65]. After the ETU process, one of the optical centers is in the ground state (or, more general, in a lower than the (2) energy state) and the other one in the up-conversion state, from which can decay radiative/non-radiatively, with rate constant  $k_3$ . The radiative route gives a photon of higher energy ( $\Delta E_{13}$ ) respect to the initial excitation gap ( $\Delta E_{12}$ ).

The development of the mathematical functions that describe the temporal evolution of the luminescence from the relevant electronic states for ETU in 1D, 2D and 3D is carried out by: (1) formulation and partial solution of differential equations for the temporal evolution of

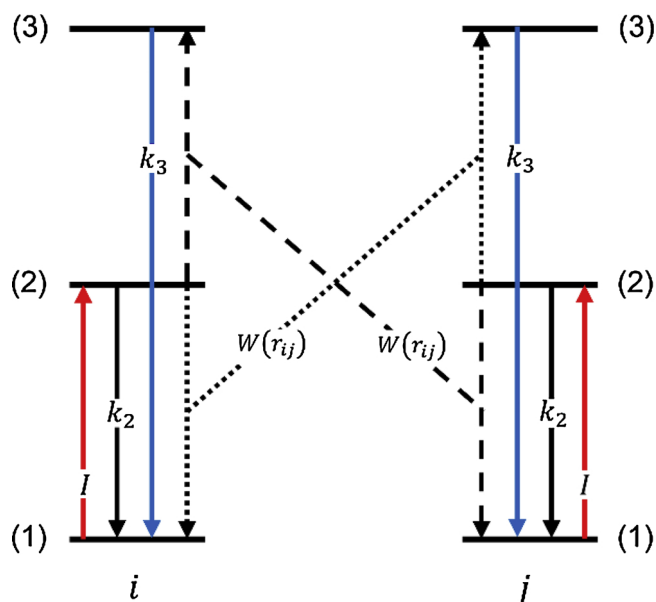


Fig. 1. Up-conversion by energy transfer process studied here. The relevant states, (1), (2), and (3), of the generic optical centers,  $i$  and  $j$ , are shown.  $I$  is the initial excitation pulse,  $k_2$  and  $k_3$  are intra-center decay rates (radiative and non-radiative intra-center processes) from states (2) and (3), respectively, and  $W(r_{ij})$  is the microscopic energy transfer rate between  $i$  and  $j$  (which can be from  $i$  to  $j$  or from  $j$  to  $i$ , as indicated by the two alternative directions).

the optical centers probabilities of being in the relevant states; (2) calculation of averages for the temporal probability of being in the intermediate state, by means of a statistical procedure based on the one of Förster [63] and Inokuti-Hirayama [65], modified for ETU and generalized to any material Euclidian dimension, and incorporating the material minimum possible distance between optical centers,  $R_m$ ; (3) development of the up-conversion time-dependent luminescence and of the macroscopic ETU rate in terms of the averaged intermediate state probability, already found in the step (2).

In addition, the model has the following implicit considerations:

- Optical centers are randomly and homogeneously distributed in the respective structure or medium, and they are static with respect to the quickness of energy transfer processes. This situation happens in doped materials, bonded optical centers, or in the so called *static limit* [17] in fluid medium.
- Optical centers are of the same electronic nature, a situation that approximately happens when optical centers are the same class of ions, molecules, etc.
- The initial excitation pulse,  $I$ , is short enough to bring the optical centers involved in the process to the intermediate state (2), without being able to populate higher energy states during the pulse duration (without any excited state absorption of pump radiation, ESAPR).
- To facilitate the study intended here, competitive ET processes, such as energy migration, retro-transference of energy, among others, will not be considered.

Even though this ETU scheme is simple, it has been observed experimentally in some materials [66–68]. It is necessary to emphasize that this simplicity is intentional to favor an easier mathematical development and to allow to reach in a direct way the main goal: studying exclusively the effect of the matrix dimensionality and the importance of the (not harmless)  $R_m$  structural parameter on the up-conversion luminescence. Future extensions of the model with other processes, such as energy migration [69], or mixed doping, will be published elsewhere. They will allow the use of the model for analysis of more realistic experimental situations.

### 2.1. Optical centers spatial distribution functions

Since the first studies of Förster [63], it has been widely and successfully used, for the general case of randomly distributed optical centers in solid (3D) matrices, the homogeneous distribution function, in which the number of optical centers that interact with a generic one increases proportionally with  $4\pi r^2/V_t$ . In this expression  $4\pi r^2$  is the area of the spherical cap of radius  $r$  (measured from the generic optical center at the origin) and  $V_t$  is the total volume of the material, which, for convenience, can be expressed as

$$V_t = u_3 R_t^3, \quad u_3 = \frac{4\pi}{3} \quad (3)$$

where  $R_t$  is the total effective spherical radius of the material, and  $u_3$  is the volume of a sphere of unit radius.

The distribution function  $4\pi r^2/V_t$  is normalized throughout the radial distance space, from  $r = 0$  to  $R_t$ . When using it to calculate the averages of the probabilities of being in the relevant states starting from  $r = 0$ , the slopes of the predicted curves at the origin of time are infinite (an approximation incorporated, for example, in Eq. (1), which is equivalent to a macroscopic (average) energy transfer rate equals to infinity at  $t = 0$ , which is a direct consequence of the Eq. (2) when  $r_{ij} = 0$ ). However, two optical centers in a real material cannot reach a mutual closest distance equal to zero, but actually the macroscopic energy transfer rate is finite at  $t = 0$ . Therefore, taking into account all of the above, it is clear that the homogeneous radial distribution functions suitable for 3D ( $n = 3$ ), 2D ( $n = 2$ ), and 1D ( $n = 1$ ) and

normalized in a radial space between  $r = R_m$  (the minimum possible distance between two optical centers) and  $r = R_t$  are:

$$F(r, n) = \begin{cases} \frac{4\pi r^2}{u_3(R_t^3 - R_m^3)} & u_3 = \frac{4\pi}{3}, \quad n = 3 \\ \frac{2\pi r^1}{u_2(R_t^2 - R_m^2)} & u_2 = \pi, \quad n = 2 \\ \frac{2r^0}{u_1(R_t - R_m)} & u_1 = 2, \quad n = 1 \end{cases} \quad (4)$$

Which, to facilitate the next subsection algebraic manipulation and results presentation, have been conveniently expressed in terms of  $u_n$ , a volume ( $n = 3$ ), area ( $n = 2$ ), or length ( $n = 1$ ) of unit radius. Expressions of Eq. (4) can be synthesized into:

$$F(r, n) = \frac{nr^{n-1}}{R_t^n - R_m^n} \quad (5)$$

which fulfills the condition

$$\int_{R_m}^{R_t} F(r, n) dr = 1 \quad (6)$$

## 2.2. Intermediate state

The temporal variation of the probability that a generic optical center  $i$  is in the intermediate state,  $p_i^{(2)}(t)$ , is described by the differential equation:

$$\frac{dp_i^{(2)}(t)}{dt} = -k_2 p_i^{(2)}(t) - 2 \sum_{j=1}^{N_t} W(r_{ij}) p_j^{(2)}(t) p_j^{(2)}(t) \quad (7)$$

where  $N_t$  is the total number of optical centers contained in the material and taking  $t = 0$  just after the pulse excitation. The partial solution of this equation is:

$$p_i^{(2)}(t) = p_i^{(2)}(0) \exp\left(-k_2 t - 2 \sum_{j=1}^{N_t} W(r_{ij}) \int_0^t p_j^{(2)}(t) dt\right) \quad (8)$$

with  $p_i^{(2)}(0)$  the probability that a generic optical center  $i$  is in the intermediate state, (2), at time  $t = 0$ . It fulfils the property:

$$\sum_{i=1}^{N_t} p_i^{(2)}(0) = N_t^{(2)}(0) = \sum_{i=1}^{N_t^{(2)}(0)} 1 \quad (9)$$

with  $N_t^{(2)}(0)$  the number of optical centers in the state (2) at time  $t = 0$ . Optical centers  $j$ , with which optical centers  $i$  interact, obey an equation of the same form as Eq. (8), which is a generic equation for any optical center. This means that  $p_i^{(2)}(t)$  is, concatenately, function of all distances among optical centers. However, it has been showed [70] that the determinant dependence is only with the main distance,  $r_{ij}$ , and that it is possible to adopt the first-order approximation:

$$p_j^{(2)}(t) \approx p_j^{(2)}(0) \exp(-k_2 t) \quad (10)$$

With this expression, Eq. (8) becomes:

$$p_i^{(2)}(t) = p_i^{(2)}(0) \exp\left(-k_2 t - 2 \sum_{j=1}^{N_t} W(r_{ij}) p_j^{(2)}(0) T(t)\right) \quad (11)$$

where

$$T(t) = \frac{1 - e^{-k_2 t}}{k_2} \quad (12)$$

To obtain the macroscopic observables, the expression for  $p_i^{(2)}(t)$  must be averaged over all the optical centers of the system:

$$\bar{p}^{(2)}(t) = \frac{1}{N_t} \sum_{i=1}^{N_t} p_i^{(2)}(0) \exp\left(-k_2 t - 2 \sum_{j=1}^{N_t} W(r_{ij}) p_j^{(2)}(0) T(t)\right) \quad (13)$$

Considering the relationship  $\bar{p}^{(2)}(0) = N_t^{(2)}(0)/N_t$  and, as indicate by Eq. (9), eliminating terms that do not contribute to the summations, we have:

$$\begin{aligned} \bar{p}^{(2)}(t) &= \frac{\bar{p}^{(2)}(0)}{N_t^{(2)}(0)} \sum_{i=1}^{N_t^{(2)}(0)} \exp\left(-k_2 t - 2 \sum_{j=1}^{N_t^{(2)}(0)} W(r_{ij}) T(t)\right) \\ &= \bar{p}^{(2)}(0) e^{-k_2 t} \frac{1}{N_t^{(2)}(0)} \sum_{i=1}^{N_t^{(2)}(0)} \left( \prod_{j=1}^{N_t^{(2)}(0)} e^{-2W(r_{ij}) T(t)} \right) \end{aligned} \quad (14)$$

The only statistical variable is the  $r_{ij}$  distance; this allows us to use a method similar to the one of Förster [63], and Inokuti-Hirayama [65] for the formulation of the  $\frac{1}{N_t^{(2)}(0)} \sum_{i=1}^{N_t^{(2)}(0)} \left( \prod_{j=1}^{N_t^{(2)}(0)} e^{-2W(r_{ij}) T(t)} \right)$  average in Eq. (14):

$$\bar{p}^{(2)}(t) = \bar{p}^{(2)}(0) e^{-k_2 t} \lim_{N_t^{(2)}(0) \rightarrow \infty} \lim_{R_t \rightarrow \infty} \left( \int_{R_m}^{R_t} F(r, n) e^{-2W(r) T(t)} dr \right)^{N_t^{(2)}(0)} \quad (15)$$

where  $F(r, n)$  is given by Eq. (5).

The integral in Eq. (15) is:

$$I_g = \int_{R_m}^{R_t} F(r, n) e^{-2W(r) T(t)} dr = \frac{n}{R_t^n - R_m^n} \int_{R_m}^{R_t} r^{n-1} e^{-\frac{K}{r^s}} dr \quad (16)$$

where Eqs. (2) and (5) have been used, and  $K = 2\Omega_s T(t)$ . Integrating by parts and making the variable change  $B = \frac{K}{r^s}$ , we have:

$$I_g = \frac{K^{-\frac{n}{s}}}{R_t^n - R_m^n} \left( B_t^{-\frac{n}{s}} e^{-B_t} - B_m^{-\frac{n}{s}} e^{-B_m} - \int_{B_t}^{B_m} B^{-\frac{n}{s}} e^{-B} dB \right) \quad (17)$$

where  $B_m = \frac{K}{R_m^s}$  and  $B_t = \frac{K}{R_t^s}$ . Writing the integral  $\int_{B_t}^{B_m} B^{-\frac{n}{s}} e^{-B} dB$  in terms of the incomplete gamma function,  $\Gamma(z, a) = \int_a^\infty B^{z-1} e^{-B} dB$ , specifying  $B_m$  and  $B_t$ , and rearranging, we have:

$$\begin{aligned} I_g &= \frac{R_t^n e^{-\frac{K}{R_t^s}} - R_m^n e^{-\frac{K}{R_m^s}}}{R_t^n - R_m^n} - \frac{K^{-\frac{n}{s}}}{R_t^n - R_m^n} \left[ \Gamma\left(1 - \frac{n}{s}, \frac{K}{R_t^s}\right) \right. \\ &\quad \left. - \Gamma\left(1 - \frac{n}{s}, \frac{K}{R_m^s}\right) \right] \end{aligned} \quad (18)$$

Using the equivalence

$$\frac{R_t^n e^{-\frac{K}{R_t^s}} - R_m^n e^{-\frac{K}{R_m^s}}}{R_t^n - R_m^n} = 1 - \frac{R_t^n (1 - e^{-\frac{K}{R_t^s}})}{R_t^n - R_m^n} - \frac{R_m^n (e^{-\frac{K}{R_m^s}} - 1)}{R_t^n - R_m^n} \quad (19)$$

and rearranging:

$$\begin{aligned} I_g &= 1 - \frac{R_t^n (1 - e^{-\frac{K}{R_t^s}})}{R_t^n - R_m^n} - \frac{1}{R_t^n - R_m^n} \left[ K^{-\frac{n}{s}} \Gamma\left(1 - \frac{n}{s}, \frac{K}{R_t^s}\right) \right. \\ &\quad \left. + R_m^n \left( e^{-\frac{K}{R_m^s}} - 1 \right) - K^{-\frac{n}{s}} \Gamma\left(1 - \frac{n}{s}, \frac{K}{R_m^s}\right) \right] \end{aligned} \quad (20)$$

Notice that

$$\frac{R_t^n \left(1 - e^{-\frac{K}{R_t^s}}\right)}{R_t^n - R_m^n} = \frac{1 - e^{-\frac{K}{R_t^s}}}{1 - \frac{R_m^n}{R_t^n}} \xrightarrow{R_t \rightarrow \infty} 0, \quad \text{and} \quad \Gamma\left(1 - \frac{n}{s}, \frac{K}{R_t^s}\right) \xrightarrow{R_t \rightarrow \infty} \Gamma\left(1 - \frac{n}{s}\right) \quad (21)$$

Furthermore, as  $N_t^{(2)}(0)$  increases when  $R_t$  increases, and the integral  $I_g$  in Eq. (15) is raised to  $N_t^{(2)}(0)$ , it is convenient to use in Eq.

(20) the equivalence (see Appendix A):

$$\frac{1}{R_t^n - R_m^n} = \frac{u_n \bar{p}_n^{(2)}(0) N_n}{N_t^{(2)}(0)} \quad (22)$$

with  $u_n$  defined in Eq. (4), and  $N_n$  is the optical centers density (optical center numerical concentration) in the  $n$ -dimensional material. Taking into account Eqs. (20),(21) and (22), the double limit of  $I_g$  in Eq. (15) is:

$$\begin{aligned} & \lim_{N_t^{(2)}(0) \rightarrow \infty} \lim_{R_t \rightarrow \infty} (I_g)^{N_t^{(2)}(0)} \\ &= \lim_{N_t^{(2)}(0) \rightarrow \infty} \left[ 1 - \frac{u_n \bar{p}_n^{(2)}(0) N_n \left[ K \frac{n}{s} \Gamma\left(1 - \frac{n}{s}\right) + R_m^n \left( e^{-\frac{K}{R_m^n}} - 1 \right) - K \frac{n}{s} \Gamma\left(1 - \frac{n}{s}, \frac{K}{R_m^n}\right) \right]}{N_t^{(2)}(0)} \right]^{N_t^{(2)}(0)} \\ &= \exp \left( -u_n \bar{p}_n^{(2)}(0) N_n \left[ K \frac{n}{s} \Gamma\left(1 - \frac{n}{s}\right) + R_m^n \left( e^{-\frac{K}{R_m^n}} - 1 \right) - K \frac{n}{s} \Gamma\left(1 - \frac{n}{s}, \frac{K}{R_m^n}\right) \right] \right) \end{aligned} \quad (23)$$

where the relationship  $\lim_{x \rightarrow \infty} \left(1 - \frac{y}{x}\right)^x = e^{-y}$  has been used. Specifying  $K = 2\Omega_s T(t)$  and reordering, the final expression for the average probability of being in the intermediate state for a material of dimension  $n$  is:

$$\begin{aligned} \bar{p}_n^{(2)}(t) &= \bar{p}_n^{(2)}(0) \times e^{-k_2 t} \times e^{-\bar{p}_n^{(2)}(0) u_n N_n \Gamma\left(1 - \frac{n}{s}\right) (2\Omega_s T(t))^{\frac{n}{s}}} \\ &\times e^{-\bar{p}_n^{(2)}(0) u_n N_n \left[ R_m^n \left( \exp\left(-\frac{2\Omega_s T(t)}{R_m^n}\right) - 1 \right) - \Gamma\left(1 - \frac{n}{s}, \frac{2\Omega_s T(t)}{R_m^n}\right) (2\Omega_s T(t))^{\frac{n}{s}} \right]} \end{aligned} \quad (24)$$

where the symbol for the dimension  $n$  has been now included in the nomenclature ( $\bar{p}_n^{(2)}(t) \equiv \bar{p}^{(2)}(t)$ ) and  $T(t)$  is given in Eq. (12).

Notice that  $\frac{\bar{p}_n^{(2)}(t)}{\bar{p}_n^{(2)}(0)} = \frac{I_n^{(2)}(t)}{I_n^{(2)}(0)}$ , where  $I_n^{(2)}(t)$  is the intensity of the intermediate state luminescence at time  $t$  in a  $n$ -dimensional material, so Eq. (24) predicts the experimental behavior. To obtain an expression in terms of the time-dependent intermediate state optical centers density,  $N_n^{(2)}(t)$ , the relationship of Eq. (25) must be considered:

$$N_n^{(stat)}(t) = \bar{p}_n^{(stat)}(t) N_n \quad (25)$$

where  $stat = (3), (2), (1)$  are the relevant states. Eq. (24) includes the correction due to the minimum possible distance between two optical centers,  $R_m$ , represented by the third exponential. It has influence on the curves slopes near  $t = 0$ , so if it is desirable studying the effect of material dimensionality on  $I_n^{(2)}(t)$  at usual time scales, it is enough to consider a simplistic version in which the third exponential is eliminated, as a consequence of making  $R_m = 0$  (classical Förster approximation):

$$\bar{p}_n^{(2)}(t) = \bar{p}_n^{(2)}(0) \times e^{-k_2 t} \times e^{-\bar{p}_n^{(2)}(0) u_n N_n \Gamma\left(1 - \frac{n}{s}\right) (2\Omega_s T(t))^{\frac{n}{s}}} \quad (26)$$

It is convenient for the subsequent analysis to express the effective interaction parameters,  $\Omega_s$ , in terms of the Förster critical transfer distance,  $R_0$  [1,63,64],

$$\Omega_s = k_2 R_0^s \quad (27)$$

This allows rewrite our final expressions in terms of the average optical centers number around a generic one,  $\nu_{n,0}$ , in a volume ( $n = 3$ ), area ( $n = 2$ ) or length ( $n = 1$ ) of  $u_n R_0^n$  Förster spatial capacity:

$$\nu_{n,0} = N_n u_n R_0^n \quad (28)$$

In this way, defining:

$$T^\vee(t) = 1 - e^{-k_2 t} \quad (29)$$

Eqs. (24) and (26) are, respectively:

$$\begin{aligned} \bar{p}_n^{(2)}(t) &= \bar{p}_n^{(2)}(0) \times e^{-k_2 t} \times e^{-\bar{p}_n^{(2)}(0) \nu_{n,0} \Gamma\left(1 - \frac{n}{s}\right) (2T^\vee(t))^{\frac{n}{s}}} \\ &\times e^{-\bar{p}_n^{(2)}(0) \nu_{n,0} \left[ \left(\frac{R_m}{R_0}\right)^n \left( \exp\left(-2\left(\frac{R_0}{R_m}\right)^s T^\vee(t)\right) - 1 \right) - \Gamma\left(1 - \frac{n}{s}, 2\left(\frac{R_0}{R_m}\right)^s T^\vee(t)\right) (2T^\vee(t))^{\frac{n}{s}} \right]} \end{aligned} \quad (30)$$

and

$$\bar{p}_n^{(2)}(t) = \bar{p}_n^{(2)}(0) \times e^{-k_2 t} \times e^{-\bar{p}_n^{(2)}(0) \nu_{n,0} \Gamma\left(1 - \frac{n}{s}\right) (2T^\vee(t))^{\frac{n}{s}}} \quad (31)$$

Notice that Eq. (31) has a mathematical form similar to Eq. (1), and that under appropriate conditions it effectively reduces to Eq. (1), as shall be.

### 2.3. Up-conversion state and macroscopic energy transfer rate

Eq. (32) describes the temporal variation for the probability that the generic optical center  $i$  is in the up-conversion state:

$$\frac{dp_i^{(3)}(t)}{dt} = -k_3 p_i^{(3)}(t) + \sum_{j=1}^{N_i} W(r_{ij}) p_i^{(2)}(t) p_j^{(2)}(t) \quad (32)$$

By using the equivalence

$$\frac{1}{u_n R_t^n} \sum_{i=1}^{N_t} p_i^{(stat)}(t) = \frac{1}{u_n R_t^n} N_t^{(stat)}(t) = N_n^{(stat)}(t) \quad (33)$$

(with  $stat = (3), (2), (1)$ , the relevant states, and  $u_n R_t^n$  the spatial capacity of the  $n$ -dimensional material, which consist in a volume,  $V_t$ , an area,  $A_t$ , or a length,  $L_t$ , for  $n = 3, 2$ , or  $1$ , respectively), and by using the following definition for the time-dependent macroscopic (average) energy transfer rate,  $W_n^{ETU}(t)$ ,

$$W_n^{ETU}(t) = \frac{1}{N_t^{(2)}(t)} \sum_{i=1}^{N_t} \sum_{j=1}^{N_t} W(r_{ij}) p_i^{(2)}(t) p_j^{(2)}(t) \quad (34)$$

differential Eq. (32) can be transformed to a one for the time-dependent up-conversion state optical center density,  $N_n^{(3)}(t)$ :

$$\frac{dN_n^{(3)}(t)}{dt} = -k_3 N_n^{(3)}(t) + W_n^{ETU}(t) N_n^{(2)}(t) \quad (35)$$

As  $N_n^{(3)}(0) = 0$ , its partial solution is:

$$N_n^{(3)}(t) = e^{-k_3 t} \int_0^t e^{k_3 t'} W_n^{ETU}(t') N_n^{(2)}(t') dt' \quad (36)$$

The macroscopic rate  $W_n^{ETU}(t)$  can be obtaining from  $N_n^{(2)}(t)$ , by previously noticing that Eq. (7) can be transformed, through Eqs. (33) and (34), to:

$$\frac{dN_n^{(2)}(t)}{dt} = -k_2 N_n^{(2)}(t) - 2W_n^{ETU}(t) N_n^{(2)}(t) \quad (37)$$

from where it follows that:

$$W_n^{ETU}(t) = -\frac{1}{2} \left( \frac{d \ln N_n^{(2)}(t)}{dt} + k_2 \right) \quad (38)$$

Using this expression in Eq. (36), integrating by parts and rearranging:

$$N_n^{(3)}(t) = \frac{N_n^{(2)}}{2} \left( e^{-k_3 t} \bar{p}_n^{(2)}(0) - \bar{p}_n^{(2)}(t) + (k_3 - k_2) e^{-k_3 t} \int_0^t e^{k_3 t'} \bar{p}_n^{(2)}(t') dt' \right) \quad (39)$$

where Eq. (25) has been used. This equation shows that  $N_n^{(3)}(t)$  can be reached from  $\bar{p}_n^{(2)}(t)$  in any of its forms, Eq. (24),(26),(30) or (31). Due to the complexity of the expressions for  $\bar{p}_n^{(2)}(t)$ , the integral that appears in Eq. (39) is only of numerical solution. An analytical approach for  $N_n^{(3)}(t)$ , is only available when  $k_3$  and  $k_2$  values are close to each other.

On the other hand, as the macroscopic energy transfer rate,  $W_n^{ETU}(t)$

(Eq. (38)), is also in terms of the averaged intermediate state quantities, it is possible to find a final expression for it. Firstly, by using Eqs. (24) and (25),  $\frac{d\ln N_n^{(2)}(t)}{dt}$  is:

$$\begin{aligned} \frac{d\ln N_n^{(2)}(t)}{dt} &= -k_2 - \bar{p}^{(2)}(0)u_n N_n \Gamma \left(1 - \frac{n}{s}\right) \left(\frac{2\Omega_s}{k_2}\right)^{\frac{n}{s}} \frac{n}{s} (1 - e^{-k_2 t})^{\frac{n}{s}-1} e^{-k_2 t} k_2 \\ &+ \bar{p}^{(2)}(0)u_n N_n R_m^n e^{-\frac{2\Omega_s}{R_m k_2} (1 - e^{-k_2 t})} \frac{2\Omega_s}{k_2 R_m^s} e^{-k_2 t} k_2 \\ &- \bar{p}^{(2)}(0)u_n N_n \frac{2\Omega_s}{R_m k_2} e^{-\frac{2\Omega_s}{R_m k_2} (1 - e^{-k_2 t}) - k_2 t} \left(\frac{2\Omega_s}{R_m k_2}\right)^{-\frac{n}{s}} (1 - e^{-k_2 t})^{-\frac{n}{s}} \\ &k_2 \left(\frac{2\Omega_s}{k_2} \{1 - e^{-k_2 t}\}\right)^{\frac{n}{s}} \\ &+ \bar{p}^{(2)}(0)u_n N_n \Gamma \left(1 - \frac{n}{s}, \frac{2\Omega_s}{R_m k_2} \{1 - e^{-k_2 t}\}\right) \left(\frac{2\Omega_s}{k_2}\right)^{\frac{n}{s}} \frac{n}{s} (1 - e^{-k_2 t})^{\frac{n}{s}-1} e^{-k_2 t} k_2 \end{aligned} \quad (40)$$

where

$$\begin{aligned} d\Gamma \left(1 - \frac{n}{s}, \frac{2\Omega_s}{R_m k_2} \{1 - e^{-k_2 t}\}\right) \\ dt \\ = -\frac{2\Omega_s}{R_m k_2} e^{-\frac{2\Omega_s}{R_m k_2} (1 - e^{-k_2 t}) - k_2 t} \left(\frac{2\Omega_s}{R_m k_2}\right)^{-\frac{n}{s}} (1 - e^{-k_2 t})^{-\frac{n}{s}} k_2 \end{aligned}$$

has been used. Simplifying Eq. (40) and reordering:

$$\begin{aligned} \frac{d\ln N_n^{(2)}(t)}{dt} &= -k_2 - \frac{\bar{p}^{(2)}(0)u_n N_n (2\Omega_s T(t))^{\frac{n}{s}} n k_2}{s(e^{k_2 t} - 1)} \left[ \Gamma \left(1 - \frac{n}{s}\right) \right. \\ &\quad \left. - \Gamma \left(1 - \frac{n}{s}, \frac{2\Omega_s}{R_m k_2} T(t)\right) \right] \end{aligned} \quad (41)$$

Therefore, Eq. (38) is:

$$\begin{aligned} W_n^{ETU}(t) &= \frac{\bar{p}^{(2)}(0)u_n N_n (2\Omega_s T(t))^{\frac{n}{s}} n k_2}{2s(e^{k_2 t} - 1)} \left[ \Gamma \left(1 - \frac{n}{s}\right) \right. \\ &\quad \left. - \Gamma \left(1 - \frac{n}{s}, \frac{2\Omega_s}{R_m k_2} T(t)\right) \right] \end{aligned} \quad (42)$$

By using Eqs. (12), (27), (28) and (29), a most suitable expression for the discussion can be reached:

$$\begin{aligned} W_n^{ETU}(t) &= \frac{\bar{p}^{(2)}(0)v_{n,0} (2\Gamma'(t))^{\frac{n}{s}} n k_2}{2s(e^{k_2 t} - 1)} \left[ \Gamma \left(1 - \frac{n}{s}\right) \right. \\ &\quad \left. - \Gamma \left(1 - \frac{n}{s}, 2\left(\frac{R_0}{R_m}\right)^s T'(t)\right) \right] \end{aligned} \quad (43)$$

As named above, due to the incorporation of a finite possible minimum distance between two optical centers,  $R_m$ , in the normalized distribution function (Eq. (6)), the macroscopic energy transfer rate is corrected from its classical infinite value ( $R_m = 0$ ) to a finite value ( $R_m > 0$ ) at  $t = 0$ . In effect, the limit of Eq. (42) or (43) when  $t \rightarrow 0$  is:

$$\lim_{t \rightarrow 0} W_n^{ETU}(t) \equiv W_n^{ETU}(0) = \frac{\bar{p}^{(2)}(0)u_n N_n \Omega_s n}{(s-n)R_m^{s-n}} = \frac{\bar{p}^{(2)}(0)v_{n,0} n k_2 R_0^{s-n}}{(s-n)R_m^{s-n}} \quad (44)$$

which is finite when  $R_m > 0$  (and infinite when  $R_m = 0$ ).

### 3. Results and discussion

Figs. 2 and 3 show semilogarithmic plots for the variation of  $\bar{p}_n^{(2)}(t)/\bar{p}_n^{(2)}(0)$  ( $n = 1, 2, 3$ ) with  $t$ , in the more exact case of Eq. (30) ( $R_m > 0$ ), for typical reference values found in Ln<sup>3+</sup>-doped amorphous solids [61,66,67,69,70], as indicated in the respective figure caption. An immediate general observation is that the curves clearly show the

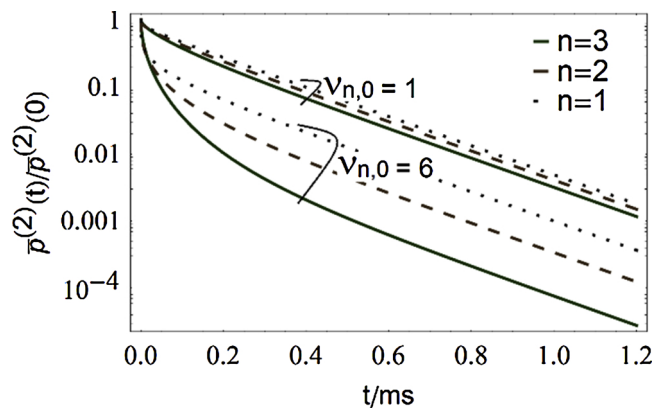


Fig. 2. Semilogarithmic plots for  $\bar{p}_n^{(2)}(t)/\bar{p}_n^{(2)}(0)$  ( $n = 1, 2, 3$ ) versus  $t$  in the case  $R_m > 0$ , Eq. (30), for  $\nu_{n,0} = 1$  and  $\nu_{n,0} = 6$ .  $R_m = 3.5 \text{ \AA}$ ,  $s = 6$ ,  $\bar{p}_n^{(2)}(0) = 0.3$ ,  $k_2 = 5.0 \text{ ms}^{-1}$ , and  $R_0 = 16.8389 \text{ \AA}$  ( $R_0$  from Eq. (28)), using  $N_3 = 5.0 \times 10^{19} \text{ cm}^{-3}$  as a reference) in all curves.

loss of simple exponential decay for the intermediate state luminescence, (2), which is a typical indicator of the energy transfer presence in randomly distributed “static” optical centers in 3D medium. As can be seen in the Figures, this effect would also be observed in 2D and 1D media. To our knowledge, there are no experimental records for the time-resolved luminescence from the energy donor or from the intermediate (initially excited) state, in the specific case of ETU in 1D and 2D media. However, it has been reported loss of simple exponential decay of the optical centers luminescence in the case of simple ET in monodoped and co-doped low dimensional materials. For example, non-exponential time-dependent emission was observed for: phthalic acid intercalated in an interlayer (2D) of Zn-Al-LDH of 1.463 nm spacing; [38] hemicyanine dye molecules located inside nanosized pores (channel diameter of 5.5 Å) of zeolite (silicalite-1) crystal [39,71], coumarin into aluminum silicate nanofilms (layer-to-layer distance of 1.4 nm) and deactivated by ET to cyanine [39,46], several organic dye molecules into the channels (diameter of 7.1 Å) of zeolite L [47–49], Gd<sup>3+</sup> aligned in a pseudo 1D K<sub>2</sub>GdF<sub>5</sub> structure in presence of the Eu<sup>3+</sup> acceptor [60] etc. Therefore, our results are similar, in the discussed sense, to these studies.

Fig. 2 shows the effect of the variation of  $\nu_{n,0}$  (the average optical centers number around a generic one within a Förster dimension, Eq. (28)). The  $\nu_{n,0}$  number is a common parameter for 1D, 2D, and 3D media that expresses the optical centers concentration, therefore, a suitable quantity to make comparisons among these three different cases. As can

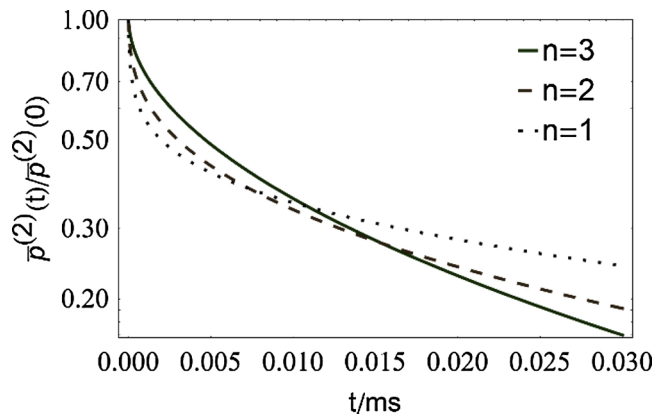


Fig. 3. Semilogarithmic plots for  $\bar{p}_n^{(2)}(t)/\bar{p}_n^{(2)}(0)$  ( $n = 1, 2, 3$ ) versus  $t$  at times close to the origin in the case  $R_m > 0$ , Eq. (30), for  $\nu_{n,0} = 6$ ,  $R_m = 3.5 \text{ \AA}$ ,  $s = 6$ ,  $\bar{p}_n^{(2)}(0) = 0.3$ ,  $k_2 = 5.0 \text{ ms}^{-1}$ , and  $R_0 = 16.8389 \text{ \AA}$  ( $R_0$  from Eq. (28)), using  $N_3 = 5.0 \times 10^{19} \text{ cm}^{-3}$  as a reference) in all curves.

be seen, when  $\nu_{n,0}$  is larger ( $\nu_{n,0} = 6$  compared with  $\nu_{n,0} = 1$  in the figure), the three respective cases, 1D, 2D, and 3D, exhibit faster decays, that is, greater deactivation in time, which, again, is an expected and typical conduct when energy transfer is present (concentration dependence) [46,48,49,71]. The same compartment, which is not showed here, is predicted with Eq. (30) for variations in  $\bar{p}_n^{(2)}(0)$ : larger  $\bar{p}_n^{(2)}(0)$  generate faster deactivation. This is a correct behavior, because  $\bar{p}_n^{(2)}(0)$  is directly proportional to the pump power excitation pulse, and the greater the intensity of the excitation pulse, the greater the concentration of active centers in the initial excited state, (2), and, therefore, faster the deactivation by energy transfer.

Likewise, as the optical centers are deactivated in time, the average distance among those that remain in the state (2) increases, which means that the energy transfer decreases (origin of the loss of simple exponential decay), and the deactivation becomes more and more of optical intra-center type, with rate  $k_2$ , so the curves approach the simple exponential decay behavior, as shown at later times in Fig. 2.

Now comparing the different Euclidean dimensions to each other in the time scale and interval showed in Fig. 2, it can be observed that 3D-distributed optical centers experiences faster deactivation than in 2D distribution, and, in turn, in 2D faster than in 1D. However, as shows Fig. 3, at times close to the origin the trend is the inverse: optical centers in smaller Euclidean dimension are deactivated faster than in larger Euclidean dimension. The curves show a crossing point between them for each pair of compared dimensions. This conduct also is the one predicted by Eq. (1) for the case of simple ET [17,53,55] but, to our knowledge there is no experimental record of it.

This behavior could be explained by the fact that at the beginning ( $t = 0$ ) the probability of having optical centers closer to each other is greater as the Euclidean dimension is smaller for the same number of optical centers in a common  $R_0$  cavity. This means that at the beginning the 1D material will be deactivated faster than the 2D ones, and these in turn faster than the 3D ones. Subsequently, at later times, due to the faster initial deactivation in the media of smaller Euclidean dimension, and with it, faster depletion of optical centers suitable for ET interaction, and also, due to the greatest number of possible directions to have optical centers with which to interact in the case of media of greater dimensionality, there will be greater number of optical centers at intermediate state with which to interact in the case of 3D with respect to 2D, and, in turn, greater in the case of 2D with respect to 1D, which means faster deactivation, respectively.

All the above results are in line with the behavior of the time-dependent macroscopic energy transfer rate,  $W_n^{ETU}(t)$ , Eqs. (42) and (43). For the interpretation we must not lose sight of the fact that  $W_n^{ETU}(t)$  reflects the averaged value for the ET interaction of a generic activated optical center to all the others activated ones that surround it, at each moment  $t$  (Eq. (34)), and that exactly corresponds to the  $\bar{p}_n^{(2)}(t)$  versus  $t$  curves slope part that originates from ET (Eq. (38)). Fig. 4 shows  $W_n^{ETU}(t)$  v/s  $t$  for the same parameters of Fig. 3, but with the time interval divided into three parts; between 0 and 0.3  $\mu\text{s}$  (Fig. 4a), between 0.3  $\mu\text{s}$  and 3  $\mu\text{s}$  (Fig. 4b), and between 3  $\mu\text{s}$  and 30  $\mu\text{s}$  (Fig. 4c). As, in this example, the optical centers concentration is high ( $\nu_{n,0} = 6$ ) and the minimum possible distance between two optical centers is rather small ( $R_m = 3.5 \text{ \AA}$ ), at  $t = 0$  the three macroscopic energy transfer rates have high (but finite) values;  $W_1^{ETU}(0) = 4640 \text{ ms}^{-1}$ ,  $W_2^{ETU}(0) = 2411 \text{ ms}^{-1}$ , and  $W_3^{ETU}(0) = 1002 \text{ ms}^{-1}$  (values indicated in the left vertical axis, Fig. 4(a), and determined with Eq. (44)). Notice that the  $W_1^{ETU}(t) > W_2^{ETU}(t) > W_3^{ETU}(t)$  trend is rapidly reversed in the next plotted time interval, Fig. 4 (b), in accordance with the indicated in Fig. 3. Notice also that, as an alternative to the physical interpretation given above, the expression of Eq. (44) allows a mathematical explanation of the fact that at the initial moments the deactivation by ET is faster for smaller Euclidean dimension: by the fact of being raised to a power of an integer greater than 1 that depends on the dimensionality of the medium ( $s - n$ ), the really determining factor of the relative magnitude of  $W_n^{ETU}(0)$  is  $(R_0/R_m)^{s-n}$  (correlatively  $\Omega_s/R_m^{s-n}$ ). As usual

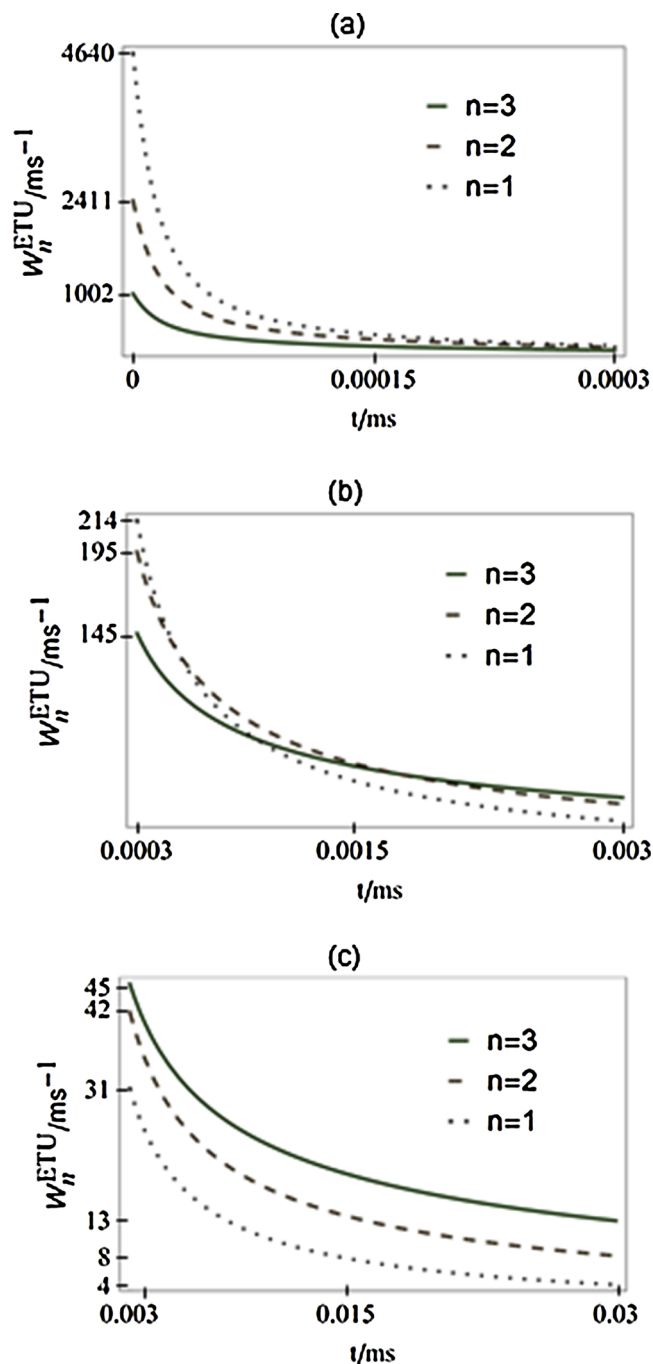
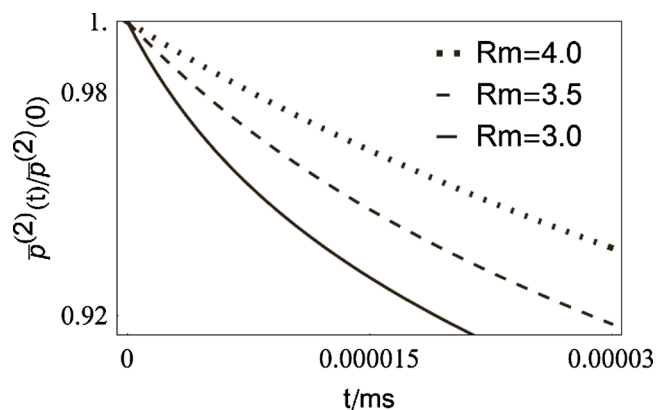


Fig. 4. Plots for  $W_n^{ETU}(t)$  ( $n = 1, 2, 3$ ) versus  $t$ , Eq. (43), for  $\nu_{n,0} = 6$ ,  $R_m = 3.5 \text{ \AA}$ ,  $s = 6$ ,  $\bar{p}_n^{(2)}(0) = 0.3$ ,  $k_2 = 5.0 \text{ ms}^{-1}$ , and  $R_0 = 16.8389 \text{ \AA}$  ( $R_0$  from Eq. (28)), using  $N_3 = 5.0 \times 10^{19} \text{ cm}^{-3}$  as a reference) in all curves. The time interval (the same of Fig. 3) was divided into: (a) 0 to 0.3  $\mu\text{s}$ , (b) 0.3 to 3  $\mu\text{s}$ , and (c) 3 to 30  $\mu\text{s}$ .

for interacting optical centers by multipolar interactions  $R_0 > R_m$ , then (as  $s - n$  is larger as the material dimensionality is smaller), the most common is that, under comparable conditions, deactivation begins faster for materials of smaller Euclidean dimensions. Finally, Fig. 4(c) shows the last plotted time interval, when  $W_3^{ETU}(t) > W_2^{ETU}(t) > W_1^{ETU}(t)$ . Notice that  $W_3^{ETU}(t)$ ,  $W_2^{ETU}(t)$ , and  $W_1^{ETU}(t)$  descends from 45, 42 and 31  $\text{ms}^{-1}$ , respectively, at 3  $\mu\text{s}$  to values comparable to  $k_2$ , 13, 8 and 4  $\text{ms}^{-1}$ , respectively, at 30  $\mu\text{s}$ , that is, at fairly early times, as can be seen when comparing with a more extended time range as showed in decay curves of Fig. 2.

On the other hand, it is interesting analyzing the effect of the



**Fig. 5.** Semilogarithmic plots for  $\bar{p}_2^{(2)}(t)/\bar{p}_2^{(2)}(0)$  versus  $t$  at times close to the origin for the cases  $R_m = 4.0 \text{ \AA}$ ,  $R_m = 3.5 \text{ \AA}$  and  $R_m = 3.0 \text{ \AA}$  (Eq. (30)). For all curves:  $\nu_{n,0} = 6$ ,  $s = 6$ ,  $\bar{p}_n^{(2)}(0) = 0.3$ ,  $k_2 = 5.0 \text{ ms}^{-1}$ , and  $R_0 = 16.8389 \text{ \AA}$  ( $R_0$  from Eq. (28)), using  $N_3 = 5.0 \times 10^{19} \text{ cm}^{-3}$  as a reference).

variation of  $R_m$  at the beginning of curves. Fig. 5 shows, in the case of 2D materials as example, that when the material structure or the characteristics of the optical centers allow that the closest possible distance between optical centers are shorter the deactivation is faster (higher initial macroscopic energy transfer rate ( $W_2^{ETU}(0) = 4467 \text{ ms}^{-1}$ ) in the  $R_m = 3.0 \text{ \AA}$  case, with respect to  $R_m = 3.5 \text{ \AA}$  case ( $W_2^{ETU}(0) = 2411 \text{ ms}^{-1}$ ), and, in turn, this last one higher than the  $R_m = 4.0 \text{ \AA}$  case ( $W_2^{ETU}(0) = 1413 \text{ ms}^{-1}$ )). These results shows that the  $R_m$  dependence incorporated in the Eq. (30) agrees with what should be expected, and the fact of having incorporated the correction for the normalization of the distribution functions (Eqs. (5) and (6)) in the deduction of the Eqs. (24) and (30), adequately corrects some incompleteness of our previous theoretical works [61,62].

Fig. 6 shows a comparison between the  $R_m > 0$  (Eq. (24) or (30)) and the  $R_m = 0$  (Eq. (26) or (31)) cases. Even though this example is for 2D, the 3D and 1D cases give similar conclusions. It can be observed that both curves show the same trend; nearly coincide, running parallel and separated by a small amount originated by the difference between the initial slopes. The latter point is shown in the details of the behavior at times close to the origin, which can be appreciated in the inserted plot. It is observed that the curve with  $R_m = 0$  (dashed curve) begins with infinite slope, while the  $R_m > 0$  one (full curve) with finite slope. As the difference between the  $R_m > 0$  and the  $R_m = 0$  cases are rather small at usual time scales, the simpler Eq. (26) or (31) can be used for most analyzes (At least for the intermediated state).

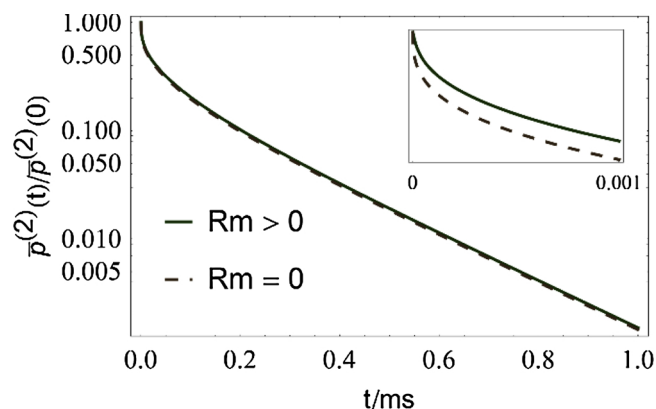


**Fig. 6.** Semilogarithmic plots for  $\bar{p}_2^{(2)}(t)/\bar{p}_2^{(2)}(0)$  (2D materials) versus  $t$  for the cases:  $R_m > 0$ , Eq. (30) (full curve), and  $R_m = 0$ , Eq. (31) (dashed curve). For both cases  $\nu_{n,0} = 3$ ,  $\bar{p}_n^{(2)}(0) = 0.3$ ,  $s = 6$ , and  $k_2 = 5.0 \text{ ms}^{-1}$ . For Eq. (30):  $R_m = 3.5 \text{ \AA}$  and  $R_0 = 16.8389 \text{ \AA}$  ( $R_0$  from Eq. (28)), using  $N_3 = 5.0 \times 10^{19} \text{ cm}^{-3}$  as a reference). The inset shows details around the beginning of time.

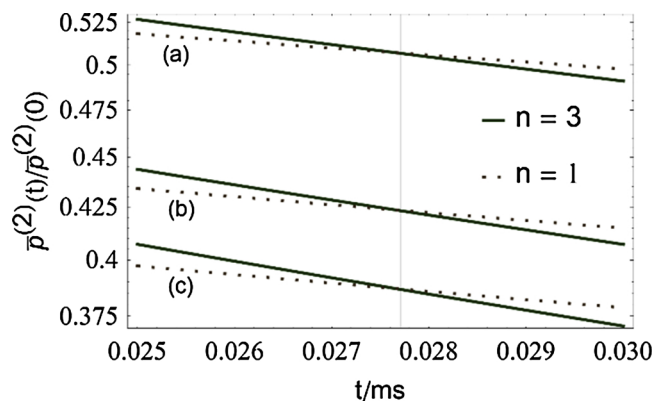


**Fig. 7.** Semilogarithmic plots of  $\bar{p}_n^{(2)}(t)/\bar{p}_n^{(2)}(0)$  versus  $t$  for Eq. (31) ( $R_m = 0$ ) in the range of intersection of the curves for  $n = 1$  and  $n = 3$ : (a)  $\nu_{n,0} = 2$  and  $\bar{p}_n^{(2)}(0) = 0.3$ , (b)  $\nu_{n,0} = 2$  and  $\bar{p}_n^{(2)}(0) = 0.4$ , and (c)  $\nu_{n,0} = 3$  and  $\bar{p}_n^{(2)}(0) = 0.3$ . For all curves  $s = 6$  and  $k_2 = 5.0 \text{ ms}^{-1}$ .

By plotting Eq. (31) for different combinations of  $\nu_{n,0}$  and  $\bar{p}_n^{(2)}(0)$  it is possible to show that the point of crossing between curves of different dimensions,  $n$ , does not depend neither on the optical centers concentration nor on excitation pump power. Fig. 7 shows three cases of  $\bar{p}_n^{(2)}(t)/\bar{p}_n^{(2)}(0)$  versus  $t$  in the range of intersection of the curves for  $n = 1$  and  $n = 3$ : (a)  $\nu_{n,0} = 2$  and  $\bar{p}_n^{(2)}(0) = 0.3$ , (b)  $\nu_{n,0} = 2$  and  $\bar{p}_n^{(2)}(0) = 0.4$ , and (c)  $\nu_{n,0} = 3$  and  $\bar{p}_n^{(2)}(0) = 0.3$ . As showed, in the three cases the curves for  $n = 1$  and  $n = 3$  intersect at the same point, indicated by means of the vertical line. This point is  $27.7 \mu\text{s}$ , which is determined by the expression:

$$t = \text{Ln} \left( 1 - \frac{1}{2} \left[ \frac{\Gamma(1 - n/s)}{\Gamma(1 - n'/s)} \right]^{\frac{s}{n-n'}} \right)^{-\frac{1}{k_2}} \quad (45)$$

Where  $n$  and  $n'$  are the involved different dimension numbers ( $n = 3$  and  $n' = 1$  in the example of Fig. 7). Eq. (45) (which is determined equaling the expression of Eq. (31) for two different cases of dimensionality,  $n$  and  $n'$ , but keeping equal the rest of the variables) clearly shows that the moment of intersection of the curves depends on  $n$ ,  $n'$ ,  $s$ , and  $k_2$ , but not on  $\nu_{n,0}$  or  $\bar{p}_n^{(2)}(0)$ . The point of intersection in the case of Eq. (30) ( $R_m > 0$ ), depends additionally on the parameters  $R_m$ , and  $R_0$ , but remains independent of  $\nu_{n,0}$  or  $\bar{p}_n^{(2)}(0)$ .

On the other hand, Fig. 8a shows the variation of the up-conversion luminescence, relative to the intermediate state luminescence at  $t = 0$ ,  $\frac{\bar{p}_n^{(3)}(t)}{\bar{p}_n^{(2)}(0)} = \frac{N_n^{(3)}(t)}{N_n^{(2)}(0)}$  (from Eq. (39), using Eq. (30) for  $\bar{p}_n^{(2)}(t)$ ), versus  $t$  for the same parameters using in Fig. 2, but for a more reduced time interval. It can be seen how at higher optical centers concentration ( $\nu_{n,0} = 6$ ) the up-conversion luminescence increases faster, reaches higher maximum values and lasts more in time with respect to lower ( $\nu_{n,0} = 1$ ) concentrations. In the curve for  $\nu_{n,0} = 6$ , it is also possible to see how the up-conversion luminescence at initial times (close to  $t = 0$ ) increases faster for smaller dimensions ( $n = 1$  faster than  $n = 2$ , and  $n = 2$  faster than  $n = 3$ ), which can also be appreciated for  $\nu_{n,0} = 1$  in a shorter time range, Fig. 8b. After the crossing among curves, the up-conversion luminescence is higher for materials of larger Euclidean dimensions, which is in line with the behavior for deactivation of the intermediate state luminescence, analyzed above. Note also how, in all cases, the final intensity for the time-resolved up-conversion luminescence reaches higher maxima and extends more in time in the case of larger dimensions. At this point, it should be clear that this behavior is for time-resolved luminescence, and not for steady-state luminescence: if the source of excitation is continuous, a constant number of excited optical centers (in the intermediate state, homogeneous and randomly distributed) will be maintained. This would mean that the number of optical centers within Förster radius,  $\nu_{n,0}$ , will remain constant in time, and if this number is the same for all the dimensions  $n$ , the probability

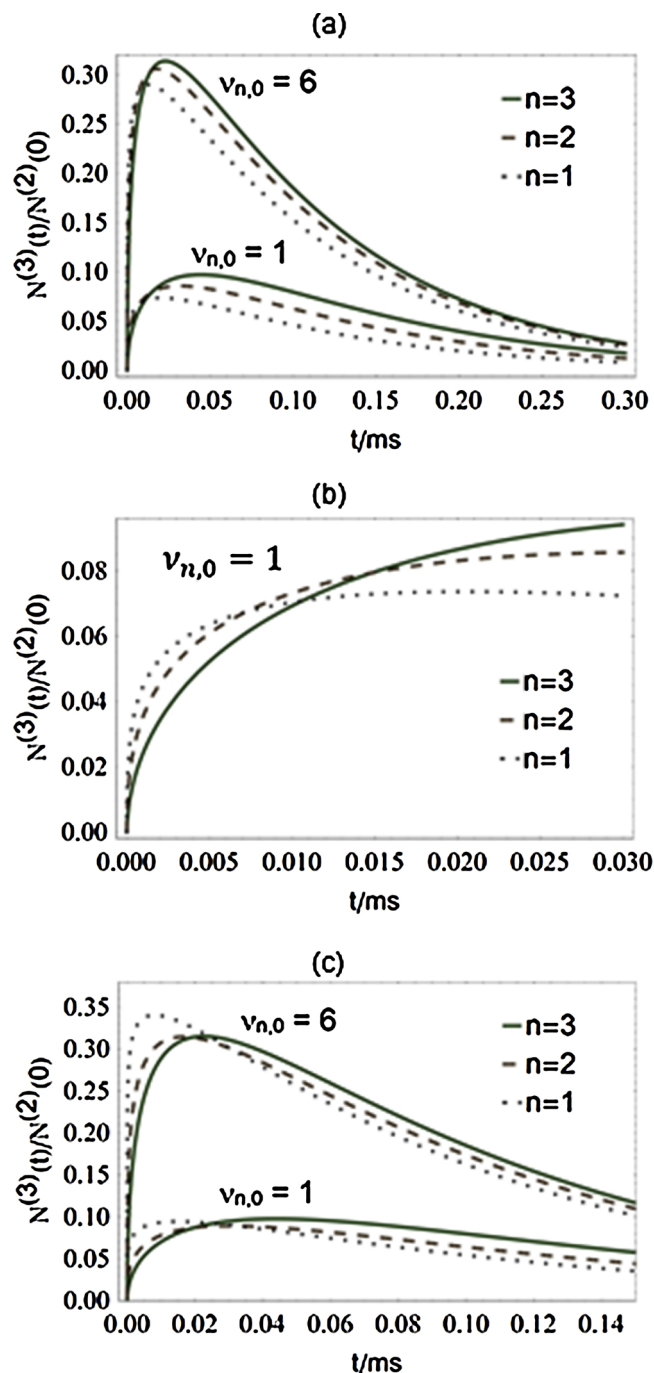


Fig. 8. Plots for  $\frac{\bar{p}_n^{(3)}(t)}{\bar{p}_n^{(2)}(0)} = \frac{N_n^{(3)}(t)}{N_n^{(2)}(0)}$  versus  $t$  (from Eq. (39)), using the same parameters of Fig. 2 and  $k_3 = 10.0 \text{ ms}^{-1}$ : (a) Using Eq. (30), case  $R_m > 0$ , for  $\bar{p}_n^{(2)}(t)$ ; (b) Details at times close to the origin for case  $v_{n,0} = 1$  of Figure (a); (c) Using Eq. (31), case  $R_m = 0$ , for  $\bar{p}_n^{(2)}(t)$  (case of wrong description).

that activated optical centers are closer to each other is greater in the

#### Appendix A. Deduction of Eq. (22)

The density of optical centers of the  $n$ -dimensional material,  $N_n$ , and the averaged probability of being in the intermediate state at  $t = 0$ ,  $\bar{p}^{(2)}(0)$ , are, respectively:

$$N_n = \frac{N_t}{u_n R_t^n}, \quad \bar{p}^{(2)}(0) = \frac{N_t^{(2)}(0)}{N_t} \quad (\text{A1})$$

where  $N_t$  and  $N_t^{(2)}(0)$  are, respectively, the absolute and the initially excited total number of optical centers in the spatial capacity,  $u_n R_t^n$ , of the  $n$ -

cases of smaller Euclidean dimensions, and therefore, one would expect that higher intensities of up-conversion luminescence in steady state regime are reached as the dimension of the material is smaller.

Finally, we must emphasize the care we must have when describing the behavior for luminescence at initial times, and the importance of incorporating the minimum approach distance,  $R_m$ , in the models for time-resolved up-conversion luminescence: Fig. 8c shows the relative up-conversion luminescence versus  $t$  for the same parameters of Fig. 8a, but using Eq. (31) for  $\bar{p}_n^{(2)}(t)$  in Eq. (39), i.e., the classical Förster  $R_m = 0$ , approximation and a shorter time interval. It is possible to see how, as a consequence of  $W_n^{ETU}(0) \rightarrow \infty$ , due to  $R_m = 0$ , the up-conversion luminescence for materials of smaller  $n$  increases much faster than the case of Fig. 8a (case with  $W_n^{ETU}(0)$  finite,  $R_m > 0$ ), to the point of retarding the moment of crossing between the curves (remember that the crossing point also depends on  $R_m$  for this case of  $R_m > 0$ ), and, with it, reaching, wrongly, absolute maxima that can even be higher in the case of smaller dimensions, with respect to cases of larger dimensions (maximum of 1D higher than 3D and 2D, in Fig. 8c).

#### 4. Conclusions

The analysis of results showed that the proposed model is completely coherent in itself (the behavior of intermediate state, up-conversion state and macroscopic ETU rate, are coherent with each other) and with what should be expected for the intermediate and up-conversion luminescence for randomly distributed “static” optical centers in 1D, 2D, or 3D medium.

The study allows to reveal that, in comparable conditions, the deactivation of the intermediate state is faster for materials of lower Euclidean dimensionality at times close to the initial ones, but that at longer times it is faster for materials of greater dimensionality. As a consequence of this the luminescence from the up-conversion state grows faster for materials of lower Euclidean dimensionality at times close to the origin ( $1D > 2D > 3D$ ), but this behavior reverses as time progresses, being faster for materials of greater dimensions ( $3D > 2D > 1D$ ), to the point of reaching higher global up-conversion intensities. The proposed physical origin for this trend allows to predict that in steady state regime the intensity of the up-conversion luminescence will be higher as the dimensionality of the medium is lower.

Finally, not taking into account the effect of the minimum possible distance of approximation between two optical centers,  $R_m$ , on the theoretical description of the up-conversion luminescence in materials of true 1, 2, and 3 dimensions, conducts to mistakes on its description.

#### Conflict of interests

The authors declare that they have no conflict of interest.

#### Acknowledgements

C. Z. H. is grateful to Universidad de Antioquia, project 2017-16239.

dimensional material. This last one can be a volume,  $V_t$ , an area,  $A_t$ , or a length,  $L_t$ , for  $n = 3, 2$ , or  $1$ , respectively,

Combining the expressions in Eq. (A1):

$$R_t^n = \frac{N_t^{(2)}(0)}{u_n N_n \bar{p}^{(2)}(0)_t} \quad (\text{A2})$$

Therefore, and due that  $R_t \gg R_m$ , one of the  $\frac{1}{R_t^n - R_m^n}$  terms in Eq. (20), can be written as:

$$\frac{1}{R_t^n - R_m^n} \cong \frac{1}{R_t^n} = \frac{u_n \bar{p}^{(2)}(0) N_n}{N_t^{(2)}(0)} \quad (\text{A4})$$

which corresponds to Eq. (22).

## References

- [1] F.E. Auzel, Materials and devices using double-pumped phosphors with energy transfer, *Proc. IEEE* 61 (1973) 758–786.
- [2] Y. Wang, K. Zheng, S. Song, D. Fan, H. Zhang, X. Liu, Remote manipulation of upconversion luminescence, *Chem. Soc. Rev.* 47 (2018) 6473–6485.
- [3] V. Gray, K. Moth-Poulsen, B. Albinsson, M. Abrahamsson, Towards efficient solid-state triplet–triplet annihilation based photon upconversion: supramolecular, macromolecular and self-assembled systems, *Coord. Chem. Rev.* 362 (2018) 54–71.
- [4] G. Lucchini, A. Speghini, P. Canton, F. Vetrone, M. Quintanilla, Engineering efficient upconverting nanothermometers using  $\text{Eu}^{3+}$  ions, *Nanoscale Adv.* 1 (2019) 757–764.
- [5] B. Gu, Q. Zhang, Recent advances on functionalized upconversion nanoparticles for detection of small molecules and ions in biosystems, *Adv. Sci.* 5 (2018), <https://doi.org/10.1002/adv.201700609>.
- [6] S. Melle, O.G. Calderón, M. Laurenti, D. Mendez-Gonzalez, A. Egatz-Gómez, E. López-Cabarcos, E. Cabrera-Granado, E. Díaz, J. Rubio-Retama, Förster resonance energy transfer distance dependence from upconverting nanoparticles to quantum dots, *J. Phys. Chem. C* 122 (2018) 18751–18758.
- [7] S. Zhu, Z. Gu, Lanthanide-Doped Materials as Dual Imaging and Therapeutic Agents, Elsevier Inc., 2018, <https://doi.org/10.1016/B978-0-12-813840-3.00011-9>.
- [8] V. Lavín, I.R. Martín, F. Lahoz, U.R. Rodríguez-Mendoza, Up-Conversion Processes in Ln(III)-doped Luminescent Materials for Photovoltaics and Photocatalysis, Elsevier Inc., 2018, <https://doi.org/10.1016/B978-0-12-813840-3.00009-0>.
- [9] B. Chen, Q. Su, W. Kong, Y. Wang, P. Shi, F. Wang, Energy transfer-based biodection using optical nanomaterials, *J. Mater. Chem. B* 6 (2018) 2924–2944.
- [10] Z. Wang, M. Hu, X. Ai, Z. Zhang, B. Xing, Near-infrared manipulation of membrane ion channels via upconversion optogenetics, *Adv. Biosyst.* (2018) 18002331800233.
- [11] L.R.P. Kassab, M.J.V. Bell, Rare-Earth-Doped Germanate and Tellurite Glasses: Laser, Waveguide, and Ultrafast Device Applications, Elsevier Inc., 2018, <https://doi.org/10.1016/B978-0-12-813840-3.00008-9>.
- [12] C. Zaldo, Lanthanide-Based Luminescent Thermosensors: From Bulk to Nanoscale, Elsevier Inc., 2018, <https://doi.org/10.1016/B978-0-12-813840-3.00010-7>.
- [13] P. Zhang, H. Chen, Y. Yang, D. Zhao, Z. Jia, K. Zheng, G. Qin, W. Qin, 3D up-conversion display of  $\text{NaYF}_4$ -PMMA covalent-linking nanocomposites, *J. Alloys Compd.* 753 (2018) 725–730.
- [14] G. Umamaheswar, G. Devarajulu, R. Megala, B. Ramesh, J.S.N.V. Ramasamy, Deva Prasad Raju, Study of optical properties and up-conversion mechanism in  $\text{Nd}^{3+}/\text{Yb}^{3+}$  ions co-doped  $\text{SiO}_2\text{-Al}_2\text{O}_3\text{-Na}_2\text{CO}_3\text{-SrF}_2\text{-CaF}_2$  glasses for green light emitting display device applications, *Optik (Stuttg)* 171 (2018) 918–924.
- [15] A.J.P. Teunissen, C. Pérez-Medina, A. Meijerink, W.J.M. Mulder, Investigating supramolecular systems using Förster resonance energy transfer, *Chem. Soc. Rev.* 47 (2018) 7027–7044.
- [16] E. Lerner, T. Cordes, A. Ingargiola, Y. Alhadid, S.Y. Chung, X. Michalet, S. Weiss, Toward dynamic structural biology: two decades of single-molecule Förster resonance energy transfer, *Science* 359 (2018), <https://doi.org/10.1126/science.aan1133>.
- [17] B. Valeur, *Molecular Fluorescence: Principles and Applications*, Wiley-VCH, Weinheim, 2001, pp. 247–272.
- [18] G. Bergamini, P. Ceroni, Metal complexes and nanoparticles for energy upconversion, *Dalton Trans.* 47 (2018) 8507–8508.
- [19] L. Ungur, Introduction to the Electronic Structure, Luminescence, and Magnetism of Lanthanides, Elsevier Inc., 2018, <https://doi.org/10.1016/B978-0-12-813840-3.00001-6>.
- [20] C. Würth, S. Fischer, B. Grauel, A.P. Alivisatos, U. Resch-Genger, Quantum yields, surface quenching, and passivation efficiency for ultrasmall core/shell upconverting nanoparticles, *J. Am. Chem. Soc.* 140 (2018) 4922–4928.
- [21] J. Li, X. Wang, Q. Zhu, B.N. Kim, X. Sun, J.G. Li, Interacting layered hydroxide nanosheets with KF leading to Y/Eu hydroxyfluoride, oxyfluoride, and complex fluoride nanocrystals and investigation of photoluminescence, *RSC Adv.* 7 (2017) 53032–53042.
- [22] Y. Li, Z. Song, L. Yao, S. Yang, Y. Zhang, Morphology/dimensionality induced tunable upconversion luminescence of  $\text{BiOCl}:\text{Yb}^{3+}/\text{Er}^{3+}$  nano/microcrystals: intense single-band red emission and underlying mechanisms, *CrystEngComm* 20 (2018) 2850–2860.
- [23] G. Cabello-Guzmán, D. González, C. Caro-Díaz, L. Lillo-Arroyo, F. Valenzuela-Melgarejo, G. Cárdenas Triviño, G.E. Buono-Core, B. Chornik, Y. Huentupil, Preliminary evaluation of the up-conversion emission of  $\text{Y}_2\text{O}_3\text{:Er-Yb}$  thin films prepared by a solid state photochemical deposition method, *J. Lumin.* 204 (2018) 401–409.
- [24] K. Fujita, R. Watanabe, Y. Iso, T. Isobe, Preparation and characterization of  $\text{Y}_2\text{O}_3\text{:Bi}^{3+},\text{Yb}^{3+}$  nanosheets with wavelength conversion from near-ultraviolet to near-infrared, *J. Lumin.* 198 (2018) 243–250.
- [25] Y. Li, Z. Song, Z. Yin, Q. Kuang, R. Wan, Y. Zhou, Q. Liu, J. Qiu, Z. Yang, Investigation on the upconversion emission in 2D  $\text{BiOBr}:\text{Yb}^{3+}/\text{Ho}^{3+}$  nanosheets, *Spectrochim. Acta - Part A Mol. Biomol. Spectrosc.* 150 (2015) 135–141.
- [26] Q. Liu, X. Yan, Y. Chen, X. Wang, Upconversion emission of  $\text{SrYbF}_5\text{:Er}^{3+}$  nanosheets modified by  $\text{Tm}^{3+}$  ions, *J. Rare Earths* 31 (2013) 1053–1058.
- [27] S. Shi, L.D. Sun, Y.X. Xue, H. Dong, K. Wu, S.C. Guo, B.T. Wu, C.H. Yan, Scalable direct writing of lanthanide-doped  $\text{KMnF}_3$  perovskite nanowires into aligned arrays with polarized upconversion emission, *Nano Lett.* 18 (2018) 2964–2969.
- [28] M. Liu, M. Gu, Y. Tian, P. Huang, L. Wang, Q. Shi, C. Cui, Multifunctional  $\text{CaSc}_2\text{O}_4\text{:Yb}^{3+}/\text{Er}^{3+}$  one-dimensional nanofibers: electrospinning synthesis and concentration-modulated upconversion luminescent properties, *J. Mater. Chem. C* 5 (2017) 4025–4033.
- [29] V. Tamilmani, A. Kumari, V.K. Rai, B. Unni Nair, K.J. Sreeram, Bright green frequency upconversion in catechin based  $\text{Yb}^{3+}/\text{Er}^{3+}$  codoped  $\text{LaVO}_4$  nanorods upon 980 nm excitation, *J. Phys. Chem. C* 121 (2017) 4505–4516.
- [30] X. Zhang, P. Yang, D. Wang, J. Xu, C. Li, S. Gai, J. Lin,  $\text{La}(\text{OH})_3\text{:Ln}^{3+}$  and  $\text{La}_2\text{O}_3\text{:Ln}^{3+}$   $\text{Ln} = \text{Yb} / \text{Er}, \text{Yb} / \text{Tm}, \text{Yb} / \text{Ho}$  microrods: Synthesis and upconversion luminescence properties, *Cryst. Growth Des.* 12 (2012) 306–312.
- [31] D. Ma, D. Yang, J. Jiang, P. Cai, S. Huang, One-dimensional hexagonal-phase  $\text{NaYF}_4$ : controlled synthesis, self-assembly, and morphology-dependent upconversion luminescence properties, *Cryst. Eng. Commun.* 12 (2010) 1650–1658.
- [32] L.A. Diaz-Torres, O. Meza, P. Salas, C. Angeles-Chavez, A. Martínez, J. Morales, J. Oliva, Dynamics of the green and red upconversion emissions in  $\text{Yb}^{3+}\text{-Er}^{3+}$ -codoped  $\text{Y}_2\text{O}_3$  nanorods, *J. Nanomater.* 2010 (2010) ID491982, <https://doi.org/10.1155/2010/491982>.
- [33] N. Song, T. Kakuta, T. aki Yamagishi, Y.W. Yang, T. Ogoshi, Molecular-scale porous materials based on pillar[n]arenes, *Chem* 4 (2018) 2029–2053.
- [34] H. Kobayashi, T. Mori, Y. Morinaga, E. Fujimori, K. Akiniwa, F. Iwahori, Electron spin resonance study of molecular orientation and dynamics of phenyl imino and nitronyl nitroxide radicals in organic 1D nanochannels of Tris(o-phenyleneedioxy) cyclotriphosphazene, *J. Phys. Chem. A* 122 (2018) 5493–5502.
- [35] Y. Kinno, H. Omachi, Y. Nakanishi, H. Shinohara, Synthesis of long-chain polythiophene inside carbon nanotubes, *Chem. Lett.* 47 (2018) 1022–1025.
- [36] D. Li, J. Wang, X. Ma, White-Light-emitting materials constructed from supramolecular approaches, *Adv. Opt. Mater.* 6 (2018) 1800273(1–27).
- [37] Y. Cui, J. Zhang, H. He, G. Qian, Photonic functional metal-organic frameworks, *Chem. Soc. Rev.* 47 (2018) 5740–5785.
- [38] R. Gao, D. Yan, Layered host-guest long-afterglow ultrathin nanosheets: high-efficiency phosphorescence energy transfer at 2D confined interface, *Chem. Sci.* 8 (2016) 590–599.
- [39] N. Alarcos, B. Cohen, M. Ziólek, A. Douhal, Photochemistry and photophysics in silica-based materials: ultrafast and single molecule spectroscopy observation, *Chem. Rev.* 117 (2017) 13639–13720.
- [40] B. Huang, Doping of RE ions in the 2D ZnO layered system to achieve low-dimensional upconverted persistent luminescence based on asymmetric doping in ZnO systems, *Phys. Chem. Chem. Phys.* 19 (2017) 12683–12711.
- [41] G. Bai, S. Yuan, Y. Zhao, Z. Yang, S.Y. Choi, Y. Chai, S.F. Yu, S.P. Lau, J. Hao, 2D layered materials of rare-earth Er-doped  $\text{MoS}_2$  with NIR-to-NIR down- and upconversion photoluminescence, *Adv. Mater.* 28 (2016) 7472–7477.
- [42] R. Sola-Llano, V. Martínez-Martínez, Y. Fujita, L. Gómez-Hortigüela, A. Alfayate, H. Uji-i, E. Fron, J. Pérez-Pariente, I. López-Arbeloa, Formation of a nonlinear optical host–guest hybrid material by tight confinement of LDS 722 into Aluminophosphate 1D nanochannels, *Chem. - A Eur. J.* 22 (2016) 15700–15711.
- [43] Z.P. Zhang, X.Y. Wang, K. Yuan, W. Zhu, T. Zhang, Y.H. Wang, J. Ke, X.Y. Zheng, C.H. Yan, Y.W. Zhang, Free-standing iridium and rhodium-based hierarchically-coiled ultrathin nanosheets for highly selective reduction of nitrobenzene to azoxybenzene under ambient conditions, *Nanoscale* 8 (2016) 15744–15752.
- [44] C. Nie, The Investigation of 1D Nanocrystals Confined in Carbon Nanotubes. Material Chemistry, Université Paul Sabatier - Toulouse III, 2016 English. NNT: 2016TOU30214.
- [45] K. Fujii, T. Kuroda, K. Sakoda, N. Iyi, Fluorescence resonance energy transfer and arrangements of fluorophores in integrated coumarin/cyanine systems within solid-state two-dimensional nanospace, *J. Photochem. Photobiol. A: Chem.* 225 (2011) 125–134.

- [46] T. Kuroda, K. Fujii, K. Sakoda, Ultrafast energy transfer in a multichromophoric layered silicate, *J. Phys. Chem. C* 114 (2010) 983–989.
- [47] C. Minkowski, R. Pansu, M. Takano, G. Calzaferri, Energy collection, transport, and trapping by a supramolecular organization of dyes in hexagonal zeolite nanocrystals, *Adv. Funct. Mater.* 16 (2006) 273–285.
- [48] M. Meyer, M.M. Yatskou, M. Pfenninger, S. Huber, G. Calzaferri, A. Digris, V. Skakun, E. Barsukov, V.V. Apanasovich, Excitation energy migration in a photonic dye-zeolite antenna: computational techniques, *J. Comput. Methods Sci. Eng.* 3 (2003) 395–402.
- [49] G. Calzaferri, S. Huber, H. Maas, C. Minkowski, Host-guest antenna materials, *Angew. Chemie - Int. Ed.* 42 (2003) 3732–3758.
- [50] C. Xu, J. Sloan, G. Brown, S. Bailey, V.C. Williams, S. Friedrichs, K.S. Coleman, E. Flahaut, J.L. Hutchison, R.E. Dunin-Borkowski, M.L.H. Green, 1D lanthanide halide crystals inserted into single-walled carbon nanotubes, *Chem. Commun.* 1 (2000) 2427–2428.
- [51] P.K. Wolber, B.S. Hudson, An analytic solution to the Förster energy transfer problem in two dimensions, *Biophys. J.* 28 (1979) 197–210.
- [52] B. Snyder, E. Freire, Fluorescence energy transfer in two dimensions. A numeric solution for random and nonrandom distributions, *Biophys. J.* 40 (1982) 137–148.
- [53] J. Klafter, A. Blumen, Fractal behavior in trapping and reaction, *J. Chem. Phys.* 80 (1984) 875–877.
- [54] J. Klafter, A. Blumen, Direct energy transfer in restricted geometries, *J. Lumin.* 34 (1985) 77–82.
- [55] J. Baumann, M.D. Fayer, Excitation transfer in disordered two-dimensional and anisotropic three-dimensional systems: effects of spatial geometry on time-resolved observables, *J. Chem. Phys.* 85 (1986) 4087–4107.
- [56] S.O. Vásquez, Energy-transfer processes in quasi-bidimensional crystal arrays, *Phys. Rev. B - Condens. Matter Mater. Phys.* 64 (1–7) (2001) 125103.
- [57] L.M.S. Loura, M. Prieto, Resonance energy transfer in heterogeneous planar and bilayer systems: theory and simulation, *J. Phys. Chem. B* 104 (2000) 6911–6919.
- [58] L.M.S. Loura, A. Fedorov, M. Prieto, Membrane probe distribution heterogeneity: a resonance energy transfer study, *J. Phys. Chem. B* 104 (2000) 6920–6931.
- [59] P.A.M. Berdowski, R. Van Mens, G. Blasse, Energy migration in a quasi-two-dimensional system:  $\text{Eu}_2\text{O}_2\text{SO}_4$ , *J. Lumin.* 33 (1985) 147–158.
- [60] R. Mahiou, J. Metin, M.T. Fournier, J.C. Cousseins, B. Jacquier, Luminescence and energy transfer in a one-dimensional compound:  $\text{K}_2\text{GdF}_5$ , *J. Lumin.* 43 (1989) 51–58.
- [61] C.Z. Hadad, Statistical approaches to the transient populations and to the macroscopic energy transfer rate for the upconversion phenomenon in monodoped amorphous solid, *J. Chem. Phys.* 127 (2007) 104711(1–10).
- [62] F. Ferraro, C.Z. Hadad, A microscopic-macroscopic analysis for mixed energy transfer schemes in doped amorphous solids, *J. Phys. Chem. A* 114 (2010) 5068–5075.
- [63] T. Förster, Experimentelle und theoretische untersuchung des zwischenmolekularen übergangs von elektronenanregungsenergie, *Zeitschrift für Naturforsch. - Sect. A, J. Phys. Sci.* 4 (1949) 321–327.
- [64] D.L. Dexter, A theory of sensitized luminescence in solids, *J. Chem. Phys.* 21 (1953) 836–850.
- [65] M. Inokuti, F. Hirayama, Influence of energy transfer by the exchange mechanism on donor luminescence, *J. Chem. Phys.* 43 (1965) 1978–1989.
- [66] E. Snoeks, G.N. Van Den Hoven, A. Polman, B. Hendriksen, M.B.J. Diemeer, F. Priolo, Cooperative upconversion in erbium-implanted soda-lime silicate glass optical waveguides, *J. Opt. Soc. Am. B* 12 (1995) 1468–1474.
- [67] T. Ohtsuki, S. Honkanen, S.I. Najafi, N. Peyghambarian, Cooperative upconversion effects on the performance of  $\text{Er}^{3+}$ -doped phosphate glass waveguide amplifiers, *J. Opt. Soc. Am. B Opt. Phys.* 14 (1997) 1838–1845.
- [68] A.L. Pelé, A. Braud, J.L. Doualan, R. Chahal, V. Nazabal, C. Boussard-Plédel, B. Bureau, R. Moncorgé, P. Camy, Wavelength conversion in  $\text{Er}^{3+}$  doped chalcogenide fibers for optical gas sensors, *Opt. Express* 23 (2015) 4163–4172.
- [69] F. Ferraro, C.Z. Hadad, Up-conversion and migration by energy transfer: a mixed model for doped luminescent solids, *J. Phys. Chem. C* 116 (2012) 7134–7143.
- [70] C.Z. Hadad, S.O. Vásquez, Statistical approach to the transient up-converted population in monodoped amorphous solids, *Phys. Chem. Chem. Phys.* 5 (2003) 3027–3033.
- [71] T.K. Shim, M.H. Lee, D. Kim, H.S. Kim, K.B. Yoon, Fluorescence characteristics of isolated dye molecules within silicalite-1 channels, *J. Fluoresc.* 22 (2012) 1475–1482.